Journal of Radiation Research, Vol. 62, No. 4, 2021, pp. 634–644
https://doi.org/10.1093/jrr/rrab030
Advance Access Publication: 31 May 2021

Dosimetry of radon progeny deposited on skin in air and thermal water

Akihiro Sakoda[1,*], Yuu Ishimori[1,2], Norie Kanzaki[1], Hiroshi Tanaka[1], Takahiro Kataoka[3], Fumihiro Mitsunobu[4] and Kiyonori Yamaoka[3]

[1]Ningyo-toge Environmental Engineering Center, Japan Atomic Energy Agency, 1550 Kamisaibara, Kagamino-cho, Tomata-gun, Okayama 708-0698, Japan
[2]Prototype Fast Breeder Reactor Monju, Japan Atomic Energy Agency, 2-1 Shiraki, Tsuruga-shi, Fukui 919-1279, Japan
[3]Graduate School of Health Sciences, Okayama University, 5-1 Shikata-cho 2-chome, Kita-ku, Okayama-shi, Okayama 700-8558, Japan
[4]Graduate School of Medicine Dentistry and Pharmaceutical Sciences, Okayama University, 5-1 Shikata-cho 2-chome, Kita-ku, Okayama-shi, Okayama 700-8558, Japan
*Corresponding author. Akihiro Sakoda, Ningyo-toge Environmental Engineering Center, Japan Atomic Energy Agency; 1550 Kamisaibara, Kagamino-cho, Tomata-gun, Okayama 708-0698, Japan; [E-mail] sakoda.akihiro@jaea.go.jp; [Tel] +81-868-44-2211; [Fax] +81-868-44-2851
(Received 27 January 2021; revised 3 March 2021; editorial decision 22 March 2021)

ABSTRACT

It is held that the skin dose from radon progeny is not negligibly small and that introducing cancer is a possible consequence under normal circumstances as there are a number of uncertainties in terms of related parameters such as activity concentrations in air and water, target cells in skin, skin covering materials, and deposition velocities. An interesting proposal has emerged in that skin exposure to natural radon-rich thermal water as part of balneotherapy can produce an immune response to induce beneficial health effects. The goal of this study was to obtain generic dose coefficients with a focus on the radon progeny deposited on the skin in air or water in relation to risk or treatment assessments. We thus first estimated the skin deposition velocities of radon progeny in air and thermal water based on data from the latest human studies. Skin dosimetry was then performed under different assumptions regarding alpha-emitting source position and target cell (i.e. basal cells or Langerhans cells). Furthermore, the impact of the radon progeny deposition on effective doses from all exposure pathways relating to 'radon exposure' was assessed using various possible scenarios. It was found that in both exposure media, effective doses from radon progeny inhalation are one to four orders of magnitude higher than those from the other pathways. In addition, absorbed doses on the skin can be the highest among all pathways when the radon activity concentrations in water are two or more orders of magnitude higher than those in air.

Keywords: radon progeny; skin; deposition velocity; air; thermal water; alpha particle

INTRODUCTION

Radon (^{222}Rn) is a natural radioactive gas that can exist anywhere in the environment and is well known to present a risk of lung cancer. In general, the pathway of so-called 'radon exposure' is the inhalation of its short-lived progeny rather than radon itself [1,2]. Arguments have also been put forward regarding other exposure pathways such as the inhalation and ingestion of radon gas [3–5], the skin permeability of radon gas [6,7], the skin deposition of radon progeny [8–12], and external exposure to radon progeny existing in air [13]. Most of these studies were focused on radiation protection, while others have been dedicated to promoting radon spa therapy research.

A fraction of the short-lived radon progeny (i.e. ^{218}Po, ^{214}Pb, ^{214}Bi, and ^{214}Po) are attached to aerosol particles in the air (known as 'attached fraction'), with the 'unattached fraction' remaining free ions. Both fractions can plate out onto any surface in the environment, including human lung airways and skin. A previous report indicated that in addition to the lungs, the deposition of the radon progeny may, under certain circumstances, lead to significant doses from alpha emitters to sensitive cells in the skin, that is, basal cell layers of between 50 and 100 μm in the skin surface [14]. Here, it has also been noted that if 70 μm is simply adopted as a nominal depth of the cell layer in accordance with the ICRP's recommendation for practically assessing

equivalent doses to locally exposed skin [15], the skin doses calculated will be negligible due to the shorter ranges of the alpha particles in skin (ca. 45 μm for ^{218}Po [6.002 MeV] and 65 μm for ^{214}Po [7.687 MeV]).

Natural radon-rich water, air, and vapor in hot springs and thermal galleys have been traditionally and successfully used for the treatment of various diseases, including rheumatism and asthma [16,17]. However, the role played by radon and/or its progeny remains controversial, with the biological mechanisms triggered by very low radiation doses resulting from such radon exposure yet to be fully elucidated. Generally, therapeutic responses are supposed to be attributed to the radiation irradiation to certain organs, tissues, and cells; however, an alternative explanation was proposed, that is, an immune response caused by irradiation to a deeper layer of the skin (e.g. Langerhans cells in the epidermis) with alpha particles from the radon progeny attached to the skin contributes to the effectiveness of that treatment [8].

For the assessment of skin doses under any conditions, the deposition velocity of the radon progeny on the skin is a key parameter that allows for predicting the skin surface activities. Two main papers have quantitatively represented the skin surface activities under given conditions, the first of which was compiled by Eatough *et al.* [12] and the second by Tempfer *et al.* [8]. In the former paper, 41 volunteers spent approximately one month wearing wristwatch alpha-particle detectors (apart from when showering or bathing) for individually monitoring the ambient activity concentrations of radon (a few to 400 Bq m^{-3}) as well as the skin surface activities of ^{218}Po and ^{214}Po. Meanwhile, in the latter paper, the skin surface activities of ^{218}Po, ^{214}Pb, ^{214}Bi, and ^{214}Po were repeatedly obtained from six volunteers during and after a 20 minute or 60 minute exposure to radon-rich thermal water (around 950 Bq l^{-1} = 950,000 Bq m^{-3}). While both studies attempted to calculate the skin doses, there was some difficultly with arbitrary exposure conditions due to the lack of information on the deposition velocity, which means that it is unfeasible to evaluate the skin dose in cases where the individual radon progeny concentrations, the attached/unattached fraction or the exposure time are different from those in these studies.

To address this issue, we first devised a methodology to estimate and optimize the deposition velocities in both air and thermal water using published empirical data [8,12]. Following this, an integrated analysis of the skin deposition was conducted and is comprehensively discussed herein. The optimized values were then used for formulating skin doses for any exposure conditions. The doses were calculated in terms of various possible scenarios for comparisons between the exposure in air and water and with doses from other exposure pathways.

MATERIALS AND METHODS

Deposition model

The change in skin surface activity of the radon progeny S_i (Bq m^{-2}) per time t (s) can be expressed as follows [8,12,18]:

$$\frac{dS_{Po-218}}{dt} = C_{Po-218}v_{Po-218} - S_{Po-218}\lambda_{Po-218} \quad (1)$$

$$\frac{dS_{Pb-214}}{dt} = C_{Pb-214}v_{Pb-214} - S_{Pb-214}\lambda_{Pb-214} + (1-k_\alpha)\,S_{Po-218}\lambda_{Pb-214} \quad (2)$$

$$\frac{dS_{Bi-214}}{dt} = C_{Bi-214}v_{Bi-214} - S_{Bi-214}\lambda_{Bi-214} + (1-k_\beta)\,S_{Pb-214}\lambda_{Bi-214} \quad (3)$$

$$S_{Po-214} = S_{Bi-214} \quad (4)$$

where C_i (Bq m^{-3}) is the concentration in air or water, v_i (m s^{-1}) is the deposition velocity, λ_i (s^{-1}) is the decay constant, k_α or k_β (−) is the fraction of desorption occurring after the alpha or beta decay of a parent nuclide, respectively and the subscript stands for a radionuclide (i = ^{218}Po, ^{214}Pb, ^{214}Bi or ^{214}Po) (see the explanation below regarding v_i, k_α and k_β). The fact that radioactive equilibrium is instantly established between ^{214}Bi and ^{214}Po due to the short half-life of ^{214}Po (164.3 μs) is the basis of equation (4) and $C_{Bi\text{-}214} = C_{Po\text{-}214}$.

Since the parameter v_i can be expected to be the same among all radon progeny [18], the relation of $v_{Po\text{-}218} = v_{Pb\text{-}214} = v_{Bi\text{-}214}$ was assumed in the case of water; however, special attention was paid to the case of air. Here, the parameter v_i was divided into two components: $v_{i,u}$ for the unattached fraction and $v_{i,a}$ for the attached fraction. Based on a previous work [18], the $v_{i,u}$ was assumed to be 100 times higher than the $v_{i,a}$. The parameters $C_{i,u}$ and $C_{i,a}$ were then defined accordingly: $C_i = C_{i,u} + C_{i,a}$. Thus, v_i can be written as:

$$v_i = \frac{C_{i,u}v_u + C_{i,a}v_a}{C_i} = \frac{v_u}{C_i}\left(C_{i,u} + \frac{C_{i,a}}{100}\right). \quad (5)$$

The parameter k_α or k_β, which can be in the range of 0–1, were incorporated into equations (2–3), based on the experimental findings: for example, if k_α or $k_\beta = 1$, S_i is not influenced by $S_{i\text{-}1}$ and is built up independently in every nuclide. In the case of air, the radon progeny (i = ^{214}Pb) can be desorbed from the material surface due to the alpha-recoil energy (much higher than the beta recoil energy) immediately after its generation by the alpha decay of the parent nuclide (i-1 = ^{218}Po) [19]. In the case of water, the radon progeny (i = ^{214}Pb or ^{214}Bi) can be readily desorbed from the material surface immediately following its generation via the decay of the parent nuclide (i-1 = ^{218}Po or ^{214}Pb, respectively), irrespective of the type of decay [8,20,21]. In the present modeling, a value of 0, 0.5 or 1 was given to k_α or k_β to evaluate the range of resulting doses. Based on the above information on desorption, different combinations of (k_α, k_β) were adopted for the different media: i.e. (0, 0) or (0.5, 0) for air and (0, 0), (0.5, 0.5) or (1, 1) for water.

Application of the deposition model to the measured data

The data used for our model application were taken from Eatough *et al.* [12] for the exposure in air and from Tempfer *et al.* [8] for the thermal water. Both the previous experiments and our application methods are described below.

(1) In air:

A total of 41 individuals participated in the one-month monitoring test. The activity concentration of radon in air ($C_{Rn\text{-}222}$) was also measured in parallel with $S_{Po\text{-}218}$ and $S_{Po\text{-}214}$ monitoring at the wrist part. The results indicated a linear relationship between $C_{Rn\text{-}222}$ and $S_{Po\text{-}218}$

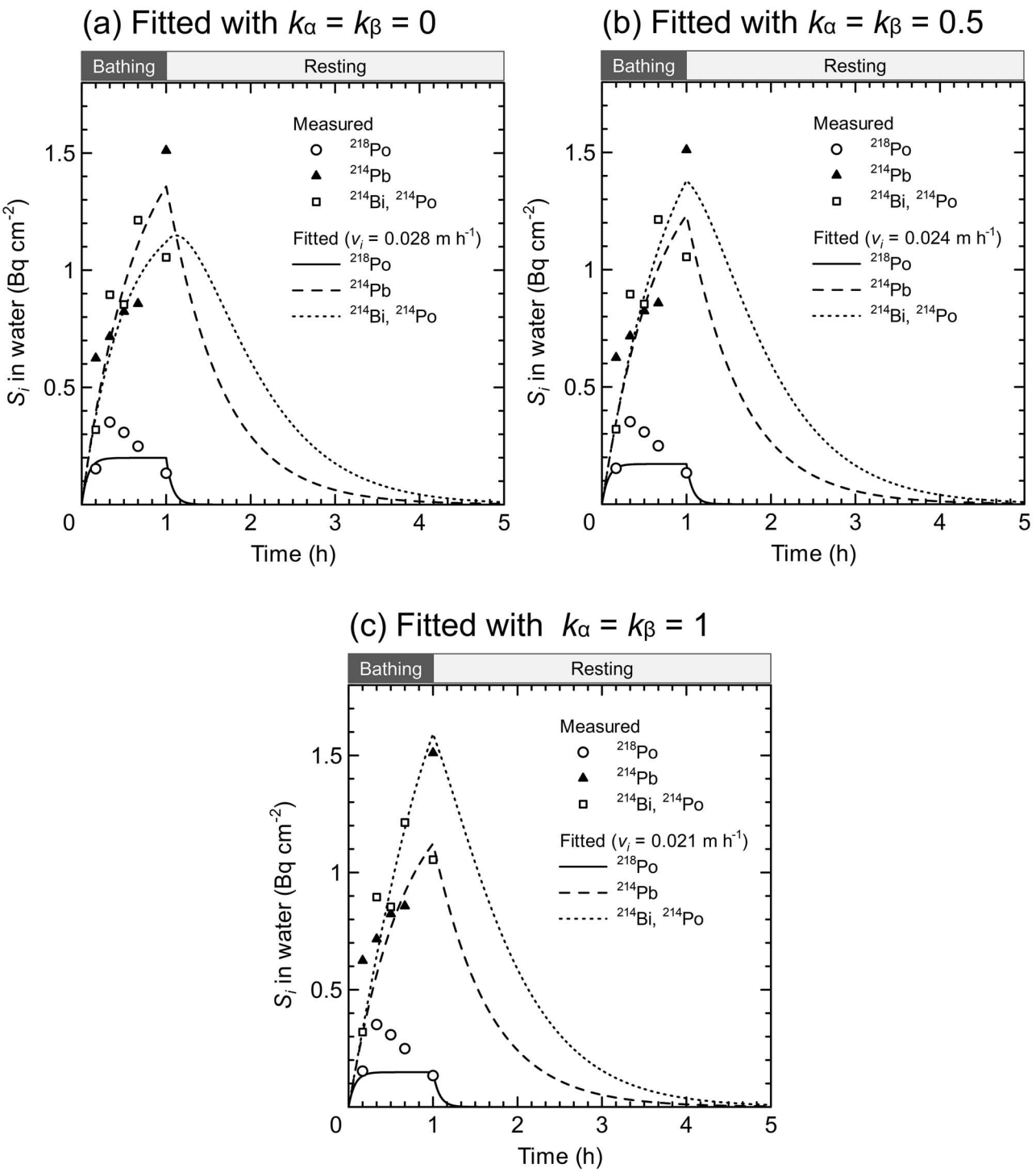

Fig. 1. Buildup and decay of the surface activities (S_i) on the skin exposed to radon-rich water ($C_{w,Rn\text{-}222}$ = 950 Bq l^{-1}). The first 60 minutes was the exposure time via bathing, whereas the remaining time was simply the resting time without exposure. The approximate relative uncertainties of the measurement were in the range of 40–90% for ^{218}Po, 10–20% for ^{214}Pb, and 10–25% for ^{214}Bi and ^{214}Po. The curves were fitted to the empirical data from Ref. [8], assuming three desorption fractions: (a) $k_\alpha = k_\beta = 0$, (b) $k_\alpha = k_\beta = 0.5$, and (c) $k_\alpha = k_\beta = 1$.

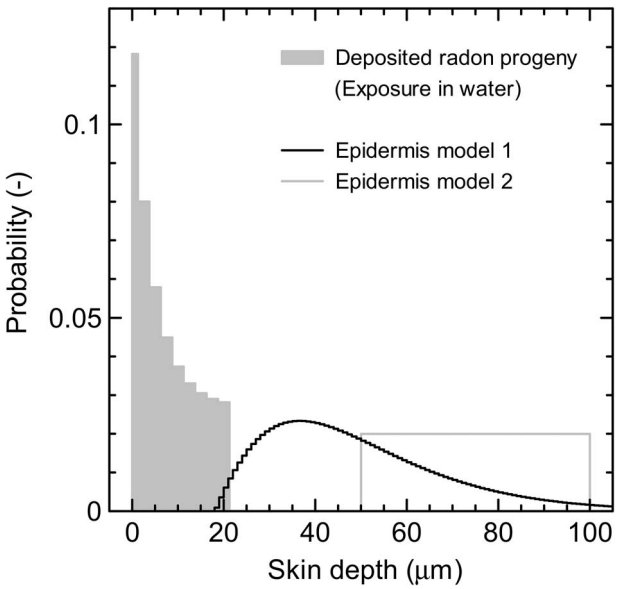

Fig. 2. Distribution of the radon progeny following the exposure via bathing and of the epidermal thickness with skin depth. In the dosimetry for the case of water, the penetration of radon progeny into skin was additionally considered according to the data drawn with gray bars [8], while the source was basically assumed to be positioned on the skin surface. The epidermis models 1 and 2 were taken from Whitton and Everall [25] and ICRP [26], respectively.

or $S_{\text{Po-214}}$. Only the data from 13 individuals were used here to obtain more appropriate values of S_i (Bq m^{-2}) per $C_{\text{Rn-222}}$ (Bq m^{-3}), i.e. and $\frac{S_{\text{Po-218}}}{C_{\text{Rn-222}}} = 0.25 \pm 0.19$ m and $\frac{S_{\text{Po-214}}}{C_{\text{Rn-222}}} = 0.22 \pm 0.11$ m.

Given that these measured values corresponded to the saturated values, the parameters v_i, $v_{i,\text{u}}$ and $v_{i,\text{a}}$ ($= v_{i,\text{u}}/100$) can be calculated under the steady state of $\frac{dS_{\text{Po-218}}}{dt} = \frac{dS_{\text{Pb-214}}}{dt} = \frac{dS_{\text{Bi-214}}}{dt} = 0$ in equations (1–3). This should be performed for a variety of possible indoor activity concentrations of the radon progeny [22]. It is reasonable to suppose indoor conditions, since all the voluntary participants were medical staff and are expected to have high occupancy factors. Thus, individual activity concentrations of the radon progeny ($C_{i,\text{a}}$ and $C_{i,\text{u}}$: i = ^{218}Po, ^{214}Pb, ^{214}Bi or ^{214}Po) that satisfy a certain equilibrium factor F of between 0.2 and 0.7 and an unattached fraction f_{p} of between 0.04 and 0.2, which were concluded as the parameter ranges of general indoor conditions in a recent international report [22], were randomly determined with 10,000 patterns under the following constraints: (a) $C_{\text{Po-218,a}} > C_{\text{Pb-214,a}} > C_{\text{Bi-214,a}}$, (b) $C_{\text{Po-218,a}} > C_{\text{Po-218,u}} > C_{\text{Pb-214,u}}$, and (c) $C_{\text{Bi-214,u}} = C_{\text{Po-214,u}} = 0$. Accordingly, 10,000 patterns of $v_{i,\text{a}}$ and $v_{i,\text{u}}$ were computed and summarized to ascertain their dependences on the assumption of F and f_{p}.

In addition, the variability analysis of $v_{i,\text{a}}$ or $v_{i,\text{u}}$ was also performed based on the Monte Carlo simulation while considering uniform distributions of F (0.2–0.7) and f_{p} (0.04–0.2) and normal distributions of $\frac{S_{\text{Po-218}}}{C_{\text{Rn-222}}}$ and $\frac{S_{\text{Po-214}}}{C_{\text{Rn-222}}}$, which generated a data set of 100,000 patterns of $C_{i,\text{a}}$ and $C_{i,\text{u}}$ that may be actually observed in an indoor environment.

(2) In water:

A total of six individuals underwent the exposure test in a thermal water bath. The activity concentration of radon in thermal water was relatively stable at $C_{\text{w,Rn-222}} = 950 \pm 73$ Bq l^{-1}, and the radon progeny was empirically verified to be in equilibrium with radon, that is, $C_{\text{w,Rn-222}} = C_{\text{w,Po-218}} = C_{\text{w,Pb-214}} = C_{\text{w,Bi-214}} = C_{\text{w,Po-214}}$. Each subject participated in several tests with different exposure times (10, 20, 30, 40 and 60 minutes). In the present work, the time-series data on $S_{\text{Po-218}}$, $S_{\text{Pb-214}}$, $S_{\text{Bi-214}}$, and $S_{\text{Po-214}}$ at the forearm part over 60 minutes were utilized for better evaluation. That is, the model of equations (1–3) was fitted to the plots in Fig. 1 to estimate v_i.

Dosimetry

The depth-dose distribution was first computed for alpha particles isotropically emitted from ^{218}Po or ^{214}Po using the particle and heavy ion transport system (PHITS) code [23]. The transport of alpha particles in a tissue-equivalent cube ($10 \times 10 \times 10$ cm^3) was simulated, and the absorbed dose was calculated by dividing the energy imparted between the depth d and $d + 1$ μm by the mass corresponding to the volume of 1 cm × 1 cm × 1 μm. The elemental composition of the skin with a density of 1.1 g cm^{-3} was taken from ICRP [24]. The source was assumed to be positioned on the skin surface, whereas in the case of the water, the skin penetration of radon progeny, which was previously indicated in Tempfer *et al.* [8], was also considered (Fig. 2).

Radiation doses to given targets that had to be set depending on the assessment purpose were then calculated with the following depth-dose distributions: (i) basal cell layer from the viewpoint of radiation risk, and (ii) Langerhans cell layer from the treatment viewpoint. The basal cells are deemed to be potentially at risk from radiation and are assumed to be positioned at the bottom layer of the epidermis [24], whereas Langerhans cells are immune cells that could play a role in indicating a positive response in the radon spa therapy [8] and are assumed to be distributed uniformly in the epidermis. Two forms of probability distribution of the basal cell layer in depth were taken from the existing literature [12,25,26] (see Fig. 2), the first of which was a relatively realistic model developed on an empirical basis (epidermis model 1), while the second was a simple model proposed for the practice of radiation protection (epidermis model 2).

Finally, absorbed dose rates to the target cells, D (μGy h^{-1} (Bq m^{-3}, ^{222}Rn)$^{-1}$), were determined as follows:

$$D = \sum_{d=1}^{r} P_d D_d \qquad \text{for basal cells} \tag{6}$$

$$D = \sum_{j=1}^{r} \left(\frac{P_j}{j} \sum_{d=1}^{j} D_d \right) \qquad \text{for Langerhans cells} \tag{7}$$

where r (μm) is the range of alpha particles in the skin, P (—) is the probability of the target cells existing at the depth d or j (μm), and D_d is the absorbed dose rate at the depth d (μm) that is available from the depth-dose distribution as calculated above.

RESULTS

Skin deposition velocity in air and water

Figure 3 shows the variation in v_{a} or v_{u} ($=100v_{\text{a}}$) for the exposure in air as a function of f_{p} between $F = 0.2$ and 0.7. Under the same F and f_{p}

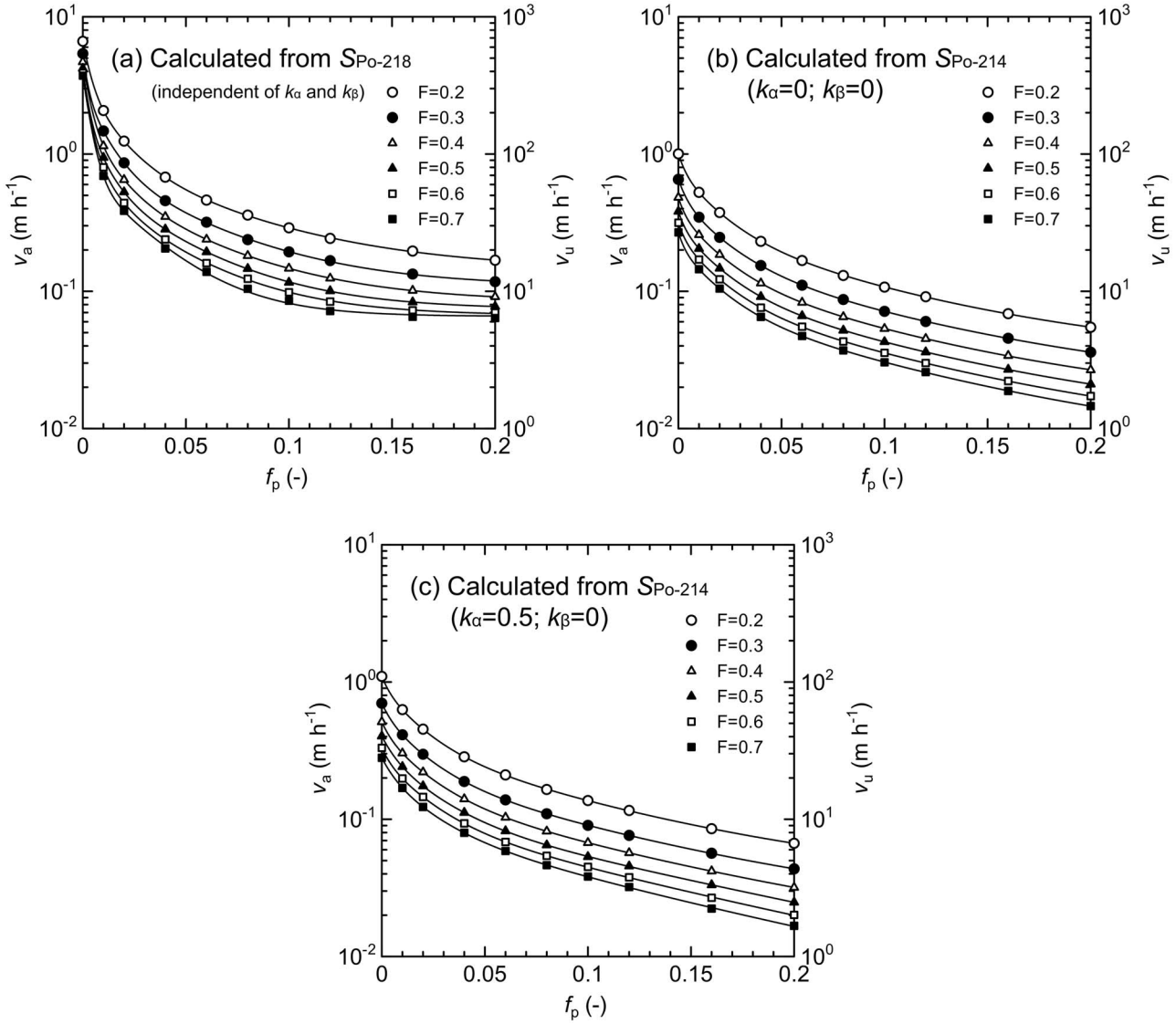

Fig. 3. Variation of the calculated skin deposition velocity of the radon progeny in air ($v_{i,a}$ or $v_{i,u}$) as a function of the assumed unattached fractions (f_p). The calculation was performed from F = 0.2 to 0.7, based on the skin surface activity (S_{Po-218} or S_{Po-214}) measured by Eatough *et al.* [12].

conditions, the plots of v_a and v_u calculated from the measured S_{Po-218} (Fig. 3a) were generally two to four times higher than those from the measured S_{Po-214} (Figs 3b,c). In addition, the plots of v_a and v_u calculated from the measured S_{Po-214} at k_α = 0.5 (Fig. 3c) were around 20% greater than those at k_α = 0 (Fig. 3b), representing relatively similar values of v_a and v_u regardless of k_α. This finding confirmed that in addition to F and f_p, the selection of the measured S_{Po-218} or S_{Po-214} was also crucial to assessing the v_a and v_u. Figure 4 shows the comparison of the variability in v_a or v_u calculated from the measured S_{Po-218} in relation to that from S_{Po-214}. In general, the explanation for the results shown in Fig. 3 also holds for those shown in Fig. 4.

Figure 1 shows the fitted curves of S_i to the measured data for the exposure in thermal water. The S_i values increased over time during the bathing with radon exposure for 1 h, with only S_{Po-218} saturated within a shorter time due to the short half-life of ^{218}Po (3.10 minutes), before the S_i values then decreased during the resting without exposure. Given its plot trend, one could suggest that S_{Po-218} reaches a maximum followed by decrease during the bathing; however, we accepted the idea of the saturation of S_{Po-218}, as the relative uncertainties of the ^{218}Po measurement were high (ca. 90% at 10 minutes, 40% at 20 and 30, 75% at 40 and 60% at 60) and a plausible mechanism producing such trend was unknown and difficult to be incorporated to the deposition model. Given the residual sum of squares, the best fit of S_{Po-218}, S_{Pb-214} and S_{Bi-214} was the case of $k_\alpha = k_\beta = 0$, and the next was that of $k_\alpha = k_\beta = 0.5$. The estimated v_i was in the range of 0.021–0.028 m h^{-1}, indicating that k_α and k_β did not significantly influence the determination of v_i.

The estimated values of v_i for both exposure in air and in water are summarized in Table 1.

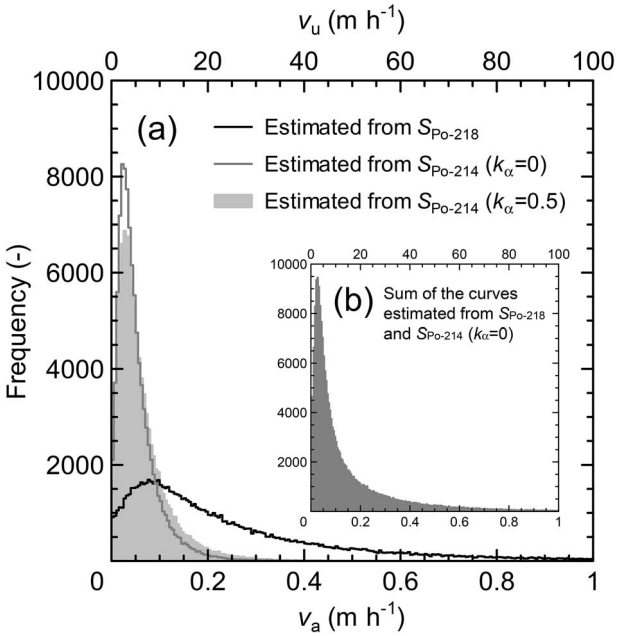

Fig. 4. Comparison of the variability in the skin deposition velocity of the radon progeny in air ($v_{i,a}$ or $v_{i,u}$) calculated from the measured $S_{Po\text{-}218}$ and $S_{Po\text{-}214}$. It should be noted that the bin ranges were different among the curves.

Skin dose

Figure 5 shows the absorbed dose rates from ^{218}Po and ^{214}Po as a function of the skin depth. Fig. 5b depicts the curves shifting to a deeper side compared with those in Fig. 5a, with approximately 15-μm longer traveling ranges for both nuclides. This indicated that the source position is influential especially when the dose imparted to a certain target that exists in the deep layer of the skin is assessed.

Figure 6 shows the absorbed doses as a function of exposure time in water, which was evaluated using two types of the epidermis models shown in Fig. 2. These doses can be obtained via the sum of $D_{Po\text{-}218}$ and $D_{Po\text{-}214}$ after integrating the dose rates D for ^{218}Po and ^{214}Po over the interval when the alpha irradiation occurs (i.e. bathing and its following rest time until the skin deposited activities reached an insignificant level). Here, it was clear that the doses were dependent on the source position, the target cell position and the epidermis model (i.e. the depth profile of the epidermis). The doses to Langerhans cells were higher (around 2× in Fig. 6a and around 10× in Fig. 6b) than those to the basal cells. Epidermis model 1, which had the targets largely at a shallower depth, induced higher doses, especially for the basal cells (around 5–8×), than epidermis model 2. The source lying only on the skin surface produced slightly higher doses (around 2× at most) than that lying between the surface to 20 μm. Meanwhile, it was noted that the desorption parameters k_α and k_β did not significantly affect the doses.

The evaluated absorbed dose rates to a specific target cell layer in the skin for both exposure in air and in water are summarized in Table 2.

Table 1. Estimated skin deposition velocity of radon progeny

Exposure medium	Desorption fraction (−)	Deposition velocity (m h^{-1})[a]		
Air [b]	$k_\alpha = 0$; $k_\beta = 0$	Estimated from the measured $S_{i,Po\text{-}218}$[c]	Estimated from the measured $S_{i,Po\text{-}214}$	Estimated from both of the measured $S_{i,Po\text{-}218}$ and $S_{i,Po\text{-}214}$
		$v_{i,a}$ = 0.18 (0.27 ± 0.29)	$v_{i,a}$ = 0.040 (0.052 ± 0.042)	$v_{i,a}$ = 0.075 (0.16 ± 0.24)
		$v_{i,u}$ = 18 (27 ± 29)	$v_{i,u}$ = 4.0 (5.2 ± 4.2)	$v_{i,u}$ = 7.5 (16 ± 24)
	$k_\alpha = 0.5$; $k_\beta = 0$		Estimated from the measured $S_{i,Po\text{-}214}$	Estimated from both of the measured $S_{i,Po\text{-}218}$ and $S_{i,Po\text{-}214}$
			$v_{i,a}$ = 0.048 (0.064 ± 0.055)	$v_{i,a}$ = 0.085 (0.17 ± 0.23)
			$v_{i,u}$ = 4.8 (6.4 ± 5.5)	$v_{i,u}$ = 8.5 (17 ± 23)
		Representative value (This work)	**Literature values for materials such as grass, paper and metal** [18]	
		$\boldsymbol{v_{i,a}}$ **= 0.08**	$\boldsymbol{v_{i,a}}$ **= 0.02**	
		$\boldsymbol{v_{i,u}}$ **= 8**	$\boldsymbol{v_{i,u}}$ **= 2**	
Water	$k_\alpha = k_\beta = 0$	v_i = 0.028		
	$k_\alpha = k_\beta = 0.5$	v_i = 0.024		
	$k_\alpha = k_\beta = 1$	v_i = 0.021		
		Representative value (This work)		
		$\boldsymbol{v_i}$ **= 0.024**		

[a] The value of $v_{i,a}$ or $v_{i,u}$ for the medium of air corresponds to a median, with an arithmetic mean ± standard deviation in parentheses (see Fig. 4).
[b] The estimation of $v_{i,a}$ and $v_{i,u}$ based on the Monte Carlo simulation was performed under the conditions of $F = 0.45 \pm 0.14$ and $f_p = 0.12 \pm 0.05$.
[c] The single value of $v_{i,a}$ or $v_{i,u}$ for both cases of $k_\alpha = 1$, and 0.5 was obtained since its calculation did not rely on the parameter k_α.

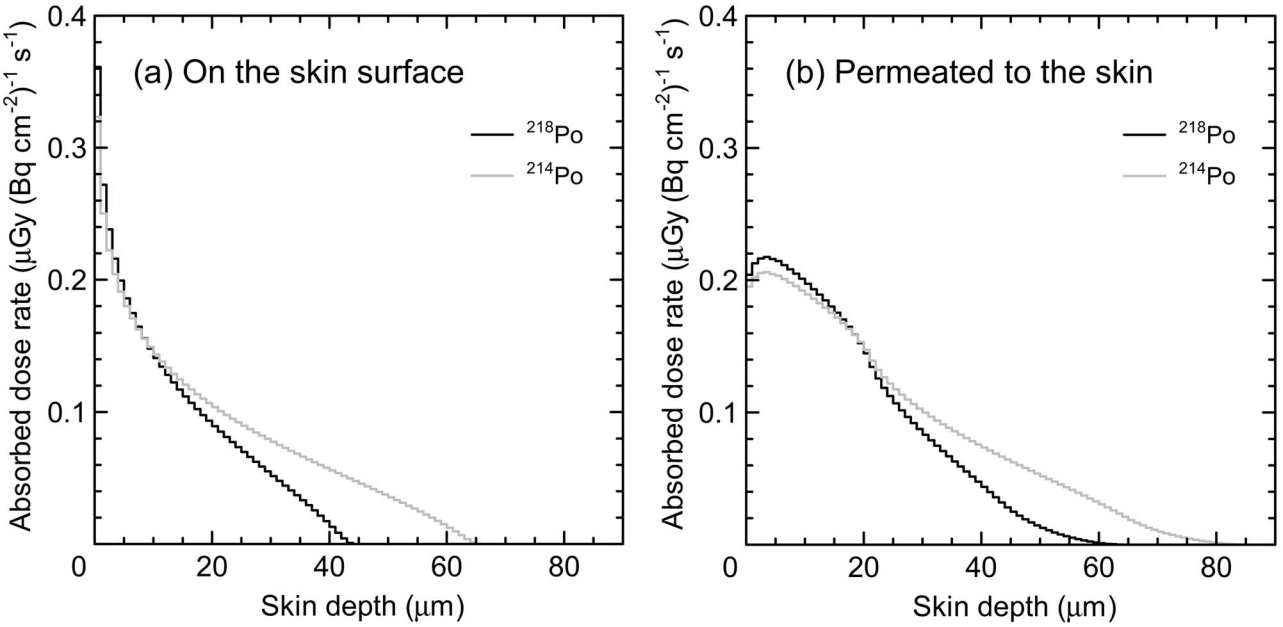

Fig. 5. Depth-dose distribution computed for alpha particles from ^{218}Po or ^{214}Po existing (a) on the skin surface or (b) from the surface to a depth of around 20 μm. The probability distribution of the deposited radon progeny in depth in terms of the case of exposure in water is presented in Fig. 2.

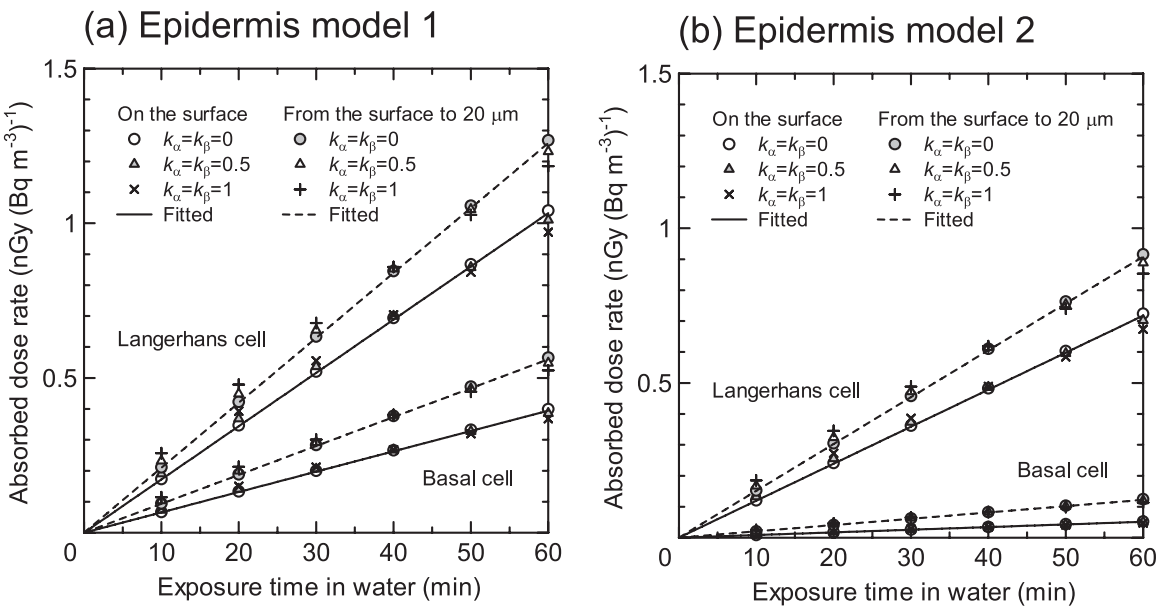

Fig. 6. Absorbed dose to a specific target cell layer as a function of time exposed in water. The epidermis models, i.e. the probability distribution of epidermis in depth, are presented in Fig. 2. The source was assumed to exist (a) on the skin surface, and (b) from the surface to 20 μm (Fig. 2). The fitted lines are numerically expressed as dose coefficients in Table 2.

DISCUSSION

Comparison of skin deposition velocities

The analysis derived $v_{i,a}$ = 0.08 and $v_{i,u}$ = 8 m h^{-1} for air and v_i = 0.024 m h^{-1} for water as representative values. The deposition velocity in water was closer to that for the attached fraction in air. It should be noted here that the conditions of the subjects in the two human studies [8,12], the data of which were used to calculate the present deposition velocities, can be expected to be quite different.

Table 2. Evaluated absorbed dose rate to a specific target cell layer in the skin

Exposure medium	Deposition velocity ($m\ h^{-1}$)	Desorption fraction (−)	Source position	Target cell	Absorbed dose rate ($nGy\ (Bq\ m^{-3}\ h,\ ^{222}Rn)^{-1}$)	
					Epidermis	
					Model 1	Model 2
Air [a]	$v_{i,a} = 0.08$; $v_{i,u} = 8$	$k_\alpha = 0$; $k_\beta = 0$	Surface	Langerhans cell	14.341	9.716
				Basal cell	4.811	0.536
Water [b]	$v_i = 0.024$	$k_\alpha = 0$; $k_\beta = 0$	Surface	Langerhans cell	1.033	0.718
				Basal cell	0.394	0.0514
			Surface to 20 μm	Langerhans cell	1.259	0.908
				Basal cell	0.560	0.122

[a] In accordance with the ICRP [27] and ICRU [22], the ratios of activity concentrations were assumed to meet the representative indoor conditions ($F = 0.4$ and $f_p = 0.08$): for the attached fraction, $C_{Rn\text{-}222} = C_{Po\text{-}218,a}$: $C_{Pb\text{-}214,a}$: $C_{Bi\text{-}214,a}$, = 1: 0.51: 0.3825: 0.306: 0.306; for the unattached fraction, $C_{Rn\text{-}222} = C_{Po\text{-}218,u}$: $C_{Pb\text{-}214,u}$: $C_{Bi\text{-}214,u}$: $C_{Po\text{-}214,u}$ = 1: 0.2: 0.02: 0: 0.

[b] The slopes of the fitted lines in Fig. 6 were equivalent to the absorbed dose rates.

For example, maybe the subjects for the bathing exposure test were sitting calmly for 60 minutes, while those for the exposure test in air were working and living as usual for a month. In short, fluid or human movement can influence the friction velocity on a surface, resulting in an increase in the chance of deposition by a factor of 3–10 [28]. Despite this influence, our findings may remain practically reasonable with regard to the similarity between $v_{i,a}$ in air and v_i in water; however, the attendant reason and mechanism cannot be explained from previously obtained experimental data.

It should also be noted that the present study assumed that $v_{i,u} = 100\ v_{i,a}$, which was based on Porstendörfer [18]. This assumption was useful and practical for the modeling but was unclear in terms of accuracy. The uncertainty of this assumption, in addition to certain other environmental parameters, could have influenced our estimation, leading to a discrepancy in the estimated $v_{i,u}$ or $v_{i,a}$ (by a factor of around 2) depending on the data source (i.e. $S_{Po\text{-}218}$, $S_{Po\text{-}214}$ or both $S_{Po\text{-}218}$ and $S_{Po\text{-}214}$) (Table 1). Further research on this topic is required to quantify the relationship between $v_{i,u}$ and $v_{i,a}$ and to improve the estimation of the skin deposition velocity of radon progeny. In addition, the impacts of aerosol particle size and air movement on the skin deposition of the radon progeny must also be better understood since the deposition velocity depends on such parameters [18,29]. The evaluation of those impacts will, in turn, contribute to improved skin dose quantification with some consideration of the environmental conditions.

The values of $v_{i,a} = 0.08$ and $v_{i,u} = 8\ m\ h^{-1}$ for the skin exposed to air were compared with those reported for specific materials (e.g., grass, filter paper and metal). Porstendörfer [18] comprehensively collated and analyzed experimental data on the deposition of radon and thoron progenies in a general room, estimating the $v_{i,a}$ value to be 0.02 and the $v_{i,u}$ value to be $2\ m\ h^{-1}$ (Table 1). This analysis was performed by considering the deposition velocities as a function of particle size, for a room with low ventilation ($<0.3\ h^{-1}$), with the assumption of the surface roughness of filter paper. Knutson [29] also provided a summary of the deposition velocity results, which presented representative average values of 0.08 and $8\ m\ h^{-1}$ for $v_{i,a}$ and $v_{i,u}$, respectively. To make a reasonable comparison between these earlier reports and this article, some attention must be given to the movement of fluid as described above. Nevertheless, it can be stated that the estimated deposition velocity to the skin will not differ greatly from that to materials such as paper and grass, when taking into account that air motion, equivalent to human motion, can enhance the deposition velocity by, at most, one order of magnitude [29].

How significantly does skin-permeating radon affect the activity measurement of the radon progeny directly deposited on the skin?

Since the intake of radon through skin from thermal water was numerically computed in a previous work [7], it was important to guarantee that there was no significant interference from the skin-permeating radon, followed by its decay, with the activity measurement of radon progeny directly deposited on the skin (Fig. 1). Without this guarantee, an implicit agreement could not be reached on how the measured data resulted solely from the skin deposition of radon progeny in water.

By means of biokinetic modeling dedicated to the skin absorption of radon [7], we quantified the buildup of radon and its progeny activity concentrations ($Bq\ kg^{-1}$) in the skin compartment during bathing in thermal water (Fig. 7). This model calculation was performed under the following conditions: $C_{w,Rn\text{-}222} = 950\ Bq\ l^{-1}$ and skin permeability coefficient $K = 1.5 \times 10^{-6}\ m\ s^{-1}$ for an adult male subject. The value of K used here corresponded to the 95th percentile of K estimated for adult males, meaning that the calculation was on the overestimated side. The calculated activity concentrations were converted to the skin surface activities ($Bq\ cm^{-2}$) by considering the approximated total (epidermis + dermis) skin mass thickness at the upper/lower arms and legs of adult males (i.e. $1.4 \times 10^{-4}\ kg\ cm^{-2}$) [24].

Finally, a comparison between Figs. 1 and 7 allowed us to conclude that in the previous experiment, the skin-permeating radon did not significantly influence the activity measurement of radon progeny deposited on the skin. Thus, the earlier measurement data taken for the present study were valid for use without correction with regard to radon permeability.

Dose assessment

Table 3 presents the effective doses for radon and its progeny exposure calculated using various given scenarios and parameter conditions. To

Table 3. Calculated effective doses from pathways relating to radon and its progeny exposures under given scenarios and parameter conditions

Scenario and condition	Effective dose (nSv (Bq m^{-3}, ^{222}Rn in air or water)$^{-1}$)			
	Radon exposure		Radon progeny exposure	
	Inhalation, $E_{Rn,inha}$	Skin permeability, $E_{Rn,skin}$	Inhalation, $E_{Rn\text{-}prog,inha}$ [a]	Skin deposition, $E_{Rn\text{-}prog,skin}$ [b]
Living environment	9.7×10^{-2}	N.A.	3.6	1.1×10^{-1}
• Medium: Air • 1-h exposure • $F = 0.4$; $f_p = 0.08$ (See the footnote of Table 2) • $v_{i,a} = 0.08$ m h^{-1}; $v_{i,u} = 8$ m h^{-1} • $k_\alpha = 0$; $k_\beta = 0$				
Thermal bath	3.2×10^{-2}	3.2×10^{-4}	1.2	3.4×10^{-3}
• Medium: Air for inhalation; Water for the skin • 20 minute exposure • $F = 0.4$ (air) or 1 (water) • $v_i = 0.024$ m h^{-1} • $k_\alpha = 0$; $k_\beta = 0$ • $K = 2.1 \times 10^{-7}$ m s^{-1} (median) [7]				

[a]The dose was calculated using a dose conversion factor of 9 nSv (Bq h m^{-3}, EEC)$^{-1}$ [30]; EEC is the abbreviation of equilibrium equivalent ^{222}Rn concentration.
[b]The source position was the skin surface, and the target was basal cells with the depth distribution of the epidermis model 2 (Fig. 2).

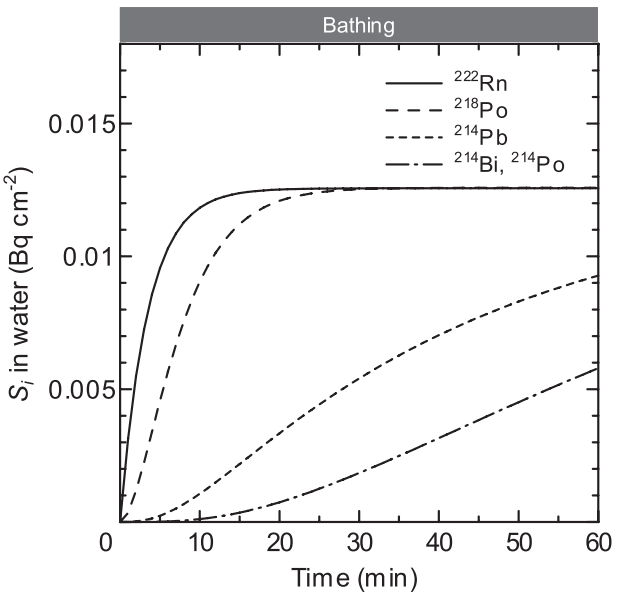

Fig. 7 Biokinetic modeling calculation of the buildup of the calculated surface activities of radon and its progeny originating from the skin permeability of radon during bathing in water ($C_{w,Rn\text{-}222}$ = 950 Bq l^{-1}).

calculate an effective dose from the absorbed dose, we used a radiation weighting factor of 20 for alpha particles and a tissue weighting factor of 0.01 for skin or 0.12 for lung [15]. Common values were used for F, f_p, and K, with the representative values concluded in this article used for v_i and the values that conservatively provide the doses used for k_α and k_β. The basal cells were set as the target and were assumed to be distributed as epidermis model 2 (Fig. 2), since this calculation targeted an effective dose that is meant to be used in relation to the risks of stochastic effects (e.g. cancer). The results clearly indicated that, for both exposure media, the effective doses from the radon progeny inhalation were much higher than those from the other pathways, i.e. by an order of magnitude in the case of air, and by two orders of magnitude (radon inhalation and radon progeny skin deposition) or four orders of magnitude (radon skin permeability) in the case of water.

Here, it should be noted that if the skin is covered with clothing or other materials, the skin deposition of the radon progeny would be suppressed so that the effective dose is reduced. As such, the doses presented in Table 3 can be qualitatively regarded as overestimated. At the same time, attention must be given to the case of exposure in water due to the possibility of a significant difference in radon activity concentration in air and water, e.g. radon spas may have a few hundred or thousands of Bq m^{-3} in air and a few hundred or thousands of kBq m^{-3} (= a few hundred or thousands of Bq l^{-1}) in water [7]. If the radon activity concentrations in a radon spa location are plausibly assumed to be 1,000 Bq m^{-3} for air and 100 kBq m^{-3} (=100 Bq l^{-1}) for water, the ratio of $E_{Rn,inha}$: $E_{Rn,skin}$: $E_{Rn\text{-}prog,inha}$: $E_{Rn\text{-}prog,skin}$ is 0.032: 0.032: 1.2: 0.34. Thus, it can be concluded that the skin deposition of

radon progeny may induce significant effective doses in certain specific cases and radon progeny inhalation is the dominant exposure pathway in daily living environments.

Thermal bathing (balneotherapy) and the resulting absorbed doses to the skin from the therapeutic viewpoint should also be considered. If the exposure time is 20 minutes and the activity concentrations of radon in air and water are 1,000 Bq m^{-3} and 100 kBq m^{-3} (=100 Bq l^{-1}), the absorbed dose to Langerhans cells can, according to Table 2, be estimated to be in the range of 24–42 μGy, while, according to Table 3, the absorbed dose to the lung (i.e. target cells relating to lung cancer) resulting from radon progeny inhalation can be estimated to be 0.5 μGy. The skin dose was found to be higher than the lung dose, while the aim of selecting the target cells is different in skin dosimetry than in lung dosimetry. This information could be valuable in scrutinizing biological/positive responses from the radon spa therapies that remain controversial and the mechanisms of which have yet to be clarified.

ACKNOWLEDGEMENTS

Akihiro Sakoda is grateful to Dr Jochen Tschiersch (Helmholtz Zentrum München, Germany) for his encouragement and support during the initiation stage of the present study.

CONFLICT OF INTEREST

The authors declare no conflicts of interest.

REFERENCES

1. Brudecki K, Li WB, Meisenberg O et al. Age-dependent inhalation doses to members of the public from indoor short-lived radon progeny. *Radiat Environ Biophys* 2014;53:535–49.
2. Sakoda A, Ishimori Y, Fukao K et al. Lung dosimetry of inhaled radon progeny in mice. *Radiat Environ Biophys* 2012;51:425–42.
3. Leggett R, Marsh J, Gregoratto D et al. A generic biokinetic model for noble gases with supplication to radon. *J Radiol Prot* 2013;33:413–32.
4. Sakoda A, Ishimori Y, Yamaoka K et al. Absorbed doses of lungs from radon retained in airway lumens of mice and rats. *Radiat Environ Biophys* 2013;52:389–95.
5. Sakoda A, Ishimori Y, Kawabe A et al. Physiologically based pharmacokinetic modeling of inhaled radon to calculate absorbed doses in mice, rats, and humans. *J Nucl Sci Technol* 2010;47:731–8.
6. Hofmann W, Winkler-Heil R, Lettner H et al. Radon transfer from thermal water to human organs in radon therapy: exhalation measurements and model simulations. *Radiat Environ Biophys* 2019;58:513–29.
7. Sakoda A, Ishimori Y, Tschiersch J. Evaluation of the intake of radon through skin from thermal water. *J Radiat Res* 2016;57:336–42.
8. Tempfer H, Hofmann W, Schober A et al. Deposition of radon progeny on skin surfaces and resulting radiation doses in radon therapy. *Radiat Environ Biophys* 2010;49:249–59.
9. Charles MW. Radon exposure of the skin: I. Biological effects. *J Radiol Prot* 2007;27:231–52.
10. Charles MW. Radon exposure of the skin: II. Estimation of the attributable risk for skin cancer incidence. *J Radiol Prot* 2007;27:253–74.
11. Falkenbach A, Kleinschmidt J, Soto J et al. Radon progeny activity on skin and hair after speleotherapeutic radon exposure. *J Environ Radioact* 2002;62:217–23.
12. Eatough JP, Worley R, Moss GR. Personal monitoring of 218Po and 214Po radionuclide deposition onto individuals under normal environmental exposure conditions. *Phys Med Biol* 1999;44:2227–39.
13. Markovic VM, Krstic D, Nikezic D et al. Doses from radon progeny as a source of external beta and gamma radiation. *Radiat Environ Biophys* 2012;51:391–7.
14. Kendall GM, Smith TJ. Doses to organs and tissues from radon and its decay products. *J Radiol Prot* 2002;22:389–406.
15. International Commission on Radiological Protection (ICRP). The 2007 recommendations of the international commission on radiological protection. ICRP publication 103. *Ann ICRP* 2007;37.
16. Maier A, Wiedemann J, Rapp F et al. Radon exposure – therapeutic effect and cancer risk. *Int J Mol Sci* 2021;22:316.
17. Mitsunobu F, Yamaoka K, Hanamoto K et al. Elevation of antioxidant enzymes in the clinical effects of radon and thermal therapy for bronchial asthma. *J Radiat Res* 2003;44:95–9.
18. Porstendörfer J. Behaviour of radon daughter products in indoor air. *Radiat Prot Dosim* 1984;7:107–13.
19. Angell CT, Pedretti M, Norman EB. Method for determining individual deposition velocities of radon progeny. *Appl Radiat Isot* 2015;98:34–9.
20. Surbeck H. Alpha spectrometry sample preparation using selectively adsorbing thin films. *Appl Radiat Isot* 2000;53:97–100.
21. Surbeck H, Andrey JL. Radon in water measurements based on thin film adsorption. In: Hunyadi I, Csige I, Hakl J (eds). *Proceedings of the 5th International Conference on Rare Gas Geochemistry*. Debrecen, Hungary, 1999, 329–34.
22. International Commission on Radiation Units and Measurements (ICRU). Measurement and reporting of radon exposures. ICRP report no. 88. *Journal of ICRU* 2012;12.
23. Sato T, Iwamoto Y, Hashimoto S et al. Features of particle and heavy ion transport code system (PHITS) version 3.02. *J Nucl Sci Technol* 2018;55:684–90.
24. International Commission on Radiological Protection (ICRP). Basic anatomical and physiological data for use in radiological protection reference values. ICRP publication 89. *Ann ICRP* 2002;32.
25. Whitton JT, Everall JD. The thickness of the epidermis. *Br J Dermatol* 1973;89:467–76.
26. International Commission on Radiological Protection (ICRP). Conversion coefficients for radiological protection quantities for external radiation exposures. ICRP publication 116. *Ann ICRP* 2010;40.
27. International Commission on Radiological Protection (ICRP). Occupational intakes of radionuclides: Part 3. ICRP publication 137. *Ann ICRP* 2017;46.
28. Bigu J. Radon daughter and thoron daughter deposition velocity and unattached fraction under laboratory-controlled conditions and in underground uranium mines. *J Aerosol Sci* 1985;16:157–165.

29. Knutson EO. Modelling indoor concentrations of radon's decay products. In: Nazaroff WW, Nero AV (eds). *Radon and its Decay Products in Indoor Air*. New York: John Wiley & Sons, 1988, 161–202.

30. United Nations Scientific Committee on the Effects of Atomic Radiation (UNSCEAR). Sources and Effects of Ionizing Radiation. In: *UNSCEAR 2000 Report to the General Assembly, with Scientific Annexes*. New York: United Nations, 2000.